



HAL
open science

New directional wave satellite observations: Towards improved wave forecasts and climate description in Southern Ocean

Lotfi Aouf, Danièle Hauser, Chapron Bertrand, A. Toffoli, C. Tourrain, C. Peureux

► To cite this version:

Lotfi Aouf, Danièle Hauser, Chapron Bertrand, A. Toffoli, C. Tourrain, et al.. New directional wave satellite observations: Towards improved wave forecasts and climate description in Southern Ocean. *Geophysical Research Letters*, 2021, e2020GL091187 (in press). 10.1029/2020GL091187 . insu-03008401v2

HAL Id: insu-03008401

<https://insu.hal.science/insu-03008401v2>

Submitted on 29 Dec 2020 (v2), last revised 15 Jun 2021 (v3)

HAL is a multi-disciplinary open access archive for the deposit and dissemination of scientific research documents, whether they are published or not. The documents may come from teaching and research institutions in France or abroad, or from public or private research centers.

L'archive ouverte pluridisciplinaire **HAL**, est destinée au dépôt et à la diffusion de documents scientifiques de niveau recherche, publiés ou non, émanant des établissements d'enseignement et de recherche français ou étrangers, des laboratoires publics ou privés.

1
2
3
4
5
6
7
8
9
10
11
12
13
14
15
16
17
18
19
20
21
22
23
24
25

New directional wave satellite observations : Towards improved wave forecasts and climate description in Southern Ocean

L. Aouf¹, D. Hauser², B. Chapron³, A. Toffoli⁴, C. Tourrain⁵, C. Peureux⁶

¹Météo-France, CNRM-DirOP, Toulouse, France

²LATMOS/IPSL, Guyancourt, France

³IFREMER, Brest, France

⁴The University of Melbourne, Melbourne, Australia

⁵CNES, Toulouse, France

⁶CLS, Brest, France

Corresponding author: Lotfi Aouf (lotfi.aouf@meteo.fr)

†Current address : Météo-France, DirOP/MAR, 42 Avenue Gaspard Coriolis Toulouse 31057 Cedex 1, France..

Key Points:

- The assimilation of directional wavenumber components in the wave model MFWAM induces a significant reduction of Significant Wave Height bias in the Southern Ocean.
- Data assimilation reveals the improvement of the energy transfer of wind waves during the wave growth phase under unlimited fetch conditions in the Pacific sector of the Southern Ocean.
- The wave age and dominant wavenumber can significantly be corrected by assimilating directional observations of SWIM, compared with assimilation of SWH-nadir only.

26 **Abstract**

27 In spite of continuous improvements of ocean wave models in the last decades, large errors still
28 remain in particular under strongly forced conditions, often encountered in the Southern Ocean,
29 where strong westerly winds generate some of the fiercest waves on Earth in almost unlimited
30 fetch conditions. The newly launched China-France Oceanography SATellite (CFOSAT)
31 provides directional spectra of ocean waves for both wind seas and swells. Compared to
32 Synthetic Aperture Radar (SAR), it can resolve shorter wavelengths in all directions, which
33 dominate in non-fully developed wind waves. Here, the assimilation of these CFOSAT wave
34 number components is proved to bring more accurate predictions of wave growth compared to
35 the assimilation of significant wave height alone. A notable reduction of model bias is found in
36 the Southern Ocean, especially in the Pacific Ocean sector. Results further exhibit a downward
37 shift of the wave age, consistent with theoretical wave growth curves.

38

39 **Plain Language Summary**

40

41 This work focuses on the importance of using directional wave observations to improve model
42 wave prediction in the Southern Ocean. The results indicate a significant impact on the transition
43 from a wind-dependent sea to a well-developed sea. A direct consequence of this work will
44 concern a better understanding of the wave climate in the Southern Ocean and therefore an
45 improvement of coupled ocean/waves/atmosphere systems.

46

47 **1 Introduction**

48 The accuracy of wave prediction models has increased notably over the past decade, following
49 the improvement of atmospheric models, which provide the wind forcing. Furthermore,
50 development of assimilation techniques has allowed the incorporation of satellite data into
51 models to optimize performances (Lionello et al, 1992). In this respect, space-borne altimeter
52 sensors provide global estimates of significant wave height—a measure of the overall energy
53 content of the wavy surface—which contributes to adjusting the variance of the wave energy
54 spectrum. Moreover, Synthetic Aperture Radar (SAR) technology provides high resolution
55 surface observations that can be converted into directional wave energy spectra. Assimilation of
56 the latter further enables a more comprehensive control of the energy density function, not only
57 allowing the optimization of the variance, but also controlling wave periods and wave directions
58 (Aouf et al, 2019). Nevertheless, SAR only robustly detects swell systems, i.e. a long wave
59 system no longer under the effect of local wind, with wavelength longer than 200 m (Collard et
60 al. 2005). The wind sea part cannot always be resolved, when propagating near along the satellite
61 direction (Chapron et al, 2001), limiting the assimilation effectiveness.

62 Generation and growth of wind sea depend on the fetch conditions (Hasselmann et al, 1973,
63 Donelan et al, 1985, Young 1999), with (nonlinear) energy transfer across wave scales, until an
64 equilibrium state (full development) is reached. More specifically, the transfer consists of an
65 inverse cascade transferring energy from high to low frequencies, which downshifts the spectral
66 peak, stretches the wavelengths and consequently accelerates the wave phase speed. Growth

67 ultimately stops, and the wind sea becomes swell, when the ratio of the wave phase speed to the
68 wind speed (i.e. wave age) is larger than about 1.2 (atmosphere cannot force waves that move
69 faster than the wind, Pierson and Moskowitz 1964, Phillips 1977). Concomitantly, there is a
70 direct cascade occurs to shift energy towards high frequencies, forcing energy to dissipate mostly
71 by wave breaking and to counterbalance the wind input.

72 Energy further re-distributes across directions so that, near the peak, the wave spectrum
73 narrowed during growth (e.g. Hasselmann et al , 1980, Donelan et al, 1985, Fadaeiazar et al.,
74 2020). The directional distribution and integrated values, such as the mean wave direction are
75 crucial parameters affecting wave growth through wind input, as the atmosphere forces energy
76 into wave components that are aligned (and almost aligned) with wind (Gunther et al, 1981).
77 However, directional properties remain one of the less known properties of the ocean surface.
78 Contemporary wave models heavily use parametrizations to shape the directional spreading
79 during the wave growth, assuming the directional distribution being unimodal (i.e. energy is
80 concentrated around one dominant direction, Hasselmann et al. 1980, Mitsuyasu et al. 1975,
81 Donelan et al. 1985) and defined by a directional spreading function of the form $\cos^{2s}(\theta)$, where
82 θ is the wave propagation direction. Today no general consensus has been reached on the exact
83 shape of the directional distribution. Moreover, field and laboratory observations have also
84 suggested that the nonlinear interactions can induce a bimodal directional distribution in the
85 early state of wave growth (Young 1995, Ewans 1998, Toffoli et al. 2010, Toffoli et al. 2017),
86 with the angle of separation among peaks depending on the wave age and wind direction (Long
87 and Resio 2006). Peaks eventually merge into a unimodal directional function consistent with
88 $\cos^{2s}(\theta)$ when approaching full development (e.g. Toffoli et al. 2017, Fadaeiazar et al., 2020).

89 Such uncertainties on the directional properties affect the identification of those wave
90 components that are aligned with the wind, and thus translate into errors in the estimation of the
91 wind input process in the wave prediction model. The extent of these errors is yet to be
92 quantified. As contemporary satellite products cannot fully optimize wind sea, the latter remains
93 a notable source of model errors, resulting in an overestimation of significant wave height
94 (positive bias). This is exacerbated in the Southern Ocean (Zieger et al. 2015)-a region covering
95 an uninterrupted band of water around Antarctica south of the main landmasses of Africa,
96 Australia, and South America—that is dominated by strong westerly winds, which blows all-the-
97 year-round with almost unlimited fetches and speed in excess of 13 m/s during summer months
98 and 18 m/s during winter months (Young et al. 2020). These intense winds generate some of the
99 fiercest waves on the planet with high percentiles of wave height exceeding 5 m during summer
100 and 7 m during winter (e.g. Babanin et al. 2019, Barbariol et al. 2019, Letraon et al. 2019, Vichi
101 et al. 2019, Young et al. 2020).

102 The newly launched China-France Oceanography Satellite (CFOSAT) carries the Surface Wave
103 Investigation Measurements (SWIM) sensor (Hauser et al. 2018) to help advance these studies.
104 Compared to SAR estimates, SWIM can resolve directional properties for a broader range of
105 wavelengths, from 70 to 500 m, to provide directional distribution of the wave energy that can
106 include both wind sea and swell systems. Here we discuss SWIM data assimilation on model
107 performance in the Southern Ocean. We demonstrate that assimilating directional properties
108 from SWIM improves prediction of energy transfer during wave growth and concurrently of
109 significant wave height. We show that model bias is reduced more efficiently when compared

110 with classical assimilation procedures that incorporate information on the significant wave height
111 only.

112 **2 CFOSAT mission and SWIM spectra**

113 The instrument SWIM of CFOSAT is a real aperture scanning radar which provides directional
114 wave spectra from several off-nadir beams (pointing at 6, 8 and 10°). Each spectrum is
115 representative of an area of about ± 35 km along-track by 90 km on each side of the nadir track,
116 and is discretized over 32 wave numbers from $[0.0126-0.279]$ rad/m, corresponding to the
117 wavelength domain $[22-500]$ m, with a geometric progression of 1.1, and 12 directions, i.e.,
118 every 15° with a 180° ambiguity in the propagation direction. During the calibration/validation
119 phase of the mission a detailed analysis was carried out (see Hauser et al. 2020). Retrieval of the
120 dominant direction, dominant wave height and significant wave height was demonstrated and
121 assessed. Except for waves propagating close to the along-track direction, 2D- wave spectra can
122 be accurately recovered over the wavelengths range of 70 to 500 m (see Hauser et al. 2020). In
123 this study, we used SWIM wave spectra derived from the most recent processing version V5.0
124 which has been shown to significantly reduce the noise impact on the detection of wave
125 partitions (see Hauser et al, 2020); furthermore, we focus on the directional wave spectra from
126 the beam 10°, demonstrated to perform the best. SWIM also provides Significant Wave Height
127 (SWH) along its track from nadir measurements (every ~ 7 km), just like the classical altimeter
128 measurement (referred to as SWIM-nadir). For the assimilation, we used observations made over
129 a 36 days period from April 26 to 1 June 2019. During this period, 343885 wave spectra from
130 SWIM were collected for the global ocean, and 95281 of which were from the Southern Ocean.

131 **3 Numerical model and data assimilation technique**

132 The MFWAM wave model describes the evolution of wave spectra in space and time
133 through the wave action conservation equation with source terms representing the wave
134 generation by the wind, the non-linear interactions and the wave breaking at sea surface. The
135 wave model MFWAM of Meteo-France is based on the IFS-ECWAM computing code of the
136 ECMWF (see IFS-38R2). The model MFWAM uses an ST4 dissipation term related to wave
137 breaking proposed by Ardhuin et al. (2010). Also, in the MFWAM model the wind input source
138 term takes into account a dissipation term due to the damping of the swell by the surface friction.
139 The non-linear interactions are represented by the Discrete Interaction Approximation (DIA)
140 which is a common approximation in numerical wave models due to its computational
141 efficiency. The MFWAM model is used for the global wave system of the Copernicus Marine
142 Service with a recent update which takes into account a spectra tail in the form of the Phillips'
143 spectrum. This parameterization is important for the calculation of the total stress provided to the
144 ocean model and the impact of waves on the atmosphere in a coupled simulation.

145 In the present study the model MFWAM uses a discretization of the wave spectrum in 24
146 directions (from 0 to 360°) and 30 frequencies increasing from 0.035Hz with a geometric
147 progression of 1.1. The MFWAM model is set for a global configuration with a grid resolution of
148 0.5°. The model is forced by analyzed winds and sea ice fraction provided by the IFS
149 atmospheric system of the ECMWF. Four sets of simulations were run : (i) with assimilation of
150 wavenumber components K_x and K_y from SWIM spectra (run A); (ii) with assimilation of
151 SWIM SWH only (run B); (iii) with assimilation of both SWH and wave number components

152 (run C); and (iv) without assimilation (run D) as a control run to examine the impact (or to build
153 a benchmark database).

154 Wavenumber components were assimilated into the model with the following scheme
155 (Aouf et al., 2006 & 2019): (i) model and SWIM spectra are partitioned to separate wind sea
156 from swell systems, following Gerling (1992); (ii) partitions of the model spectra are matched
157 with the SWIM counterpart by minimizing their Cartesian distance between their mean
158 wavenumbers. This cross-assignment process removes the SWIM partitions affected by the
159 ambiguity of 180° and also avoids including corrupted partitions; (iii) an optimal interpolation
160 between model and observations is applied to the two wavenumber components K_x and K_y of
161 each partition mean wave number; and (iv) analyzed partitions are superposed to reconstruct the
162 analyzed wave spectrum, with smoothing procedure to avoid gaps between partitions. Only
163 modes with wavelengths greater than 70 m were used for the assimilation, while the first guess
164 wave spectrum from the model stays unchanged otherwise.

165 The assimilation of SWH from SWIM instrument at nadir look consists in solely performing
166 only the optimal interpolation scheme for SWH (as a stand-alone procedure or in conjunction
167 with the assimilation of wavenumber components). Note, however, that assimilation of SWH
168 further requires a scaling of the wave spectrum in the frequency range by using the empirical
169 power laws developed in Lionello et al. (1992). This is the classical approach, used in most
170 operational models (see Aouf and Lefevre 2015).

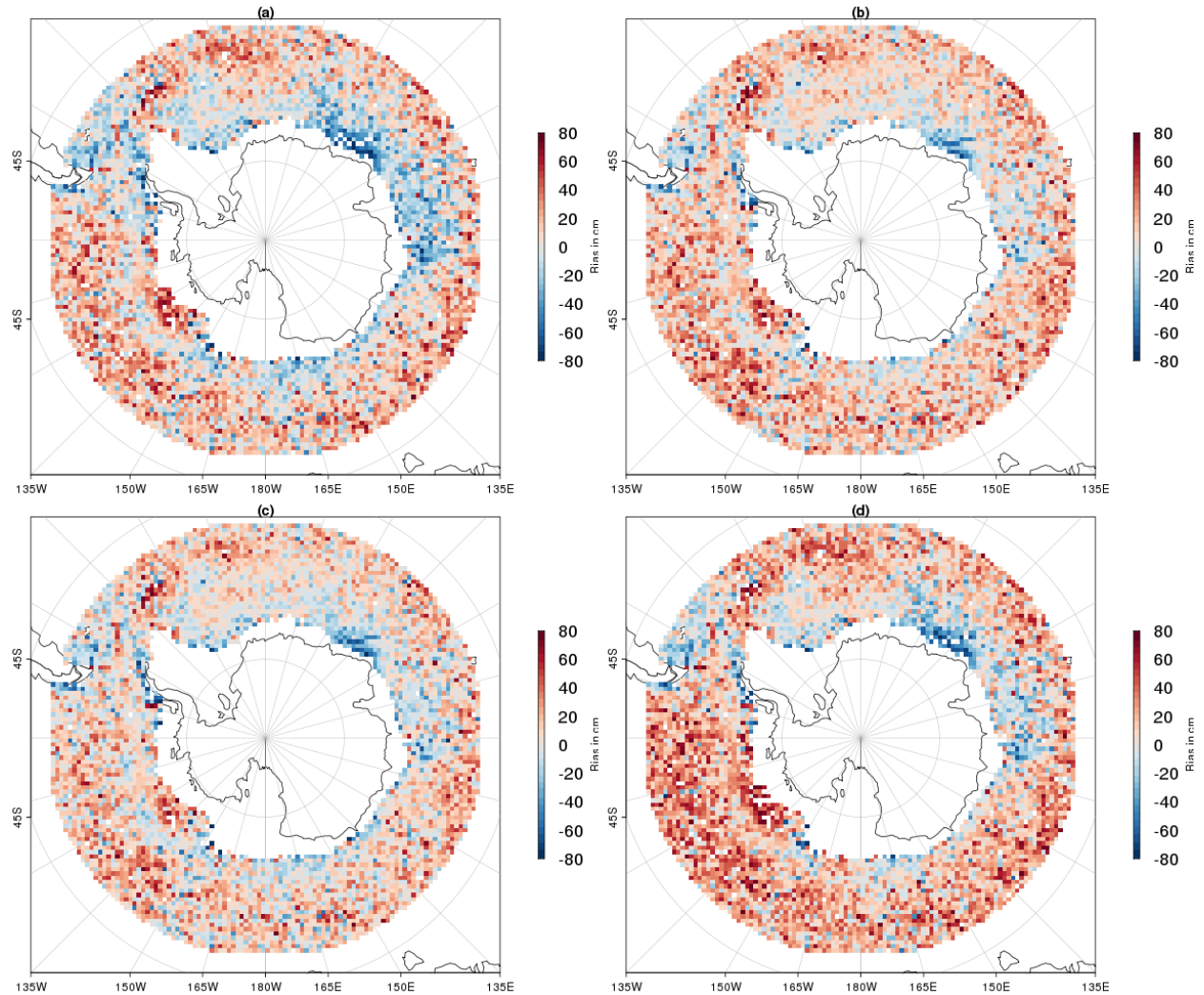
171 The study area focuses on the Southern Ocean where a large number of storm events with strong
172 winds are generated during the Austral winter. We should remark that during the period of study
173 surface wind speeds exceeding 20 m/s represent 30% for the Pacific Southern Ocean between the
174 longitudes 150°E - 250°E .

175 The Southern Ocean is well covered by altimeter missions. Therefore, the validation of
176 the model simulations is based on significant wave heights provided by the Jason-3, Saral/AltiKa
177 and Sentinel-3 altimetry missions in this region. Super-observations of SWH from altimeters
178 have been generated on the grid size of the model, which is $0.5^\circ \times 0.5^\circ$, with about 665249
179 collected points. Thus, to evaluate the impact of assimilation, we compare SWH from the four
180 model runs with those provided by the altimeters on this grid size.
181

182 **4 Results**

183 Biases on SWH from the model runs, with respect to the independent altimeter data, are
184 presented in Fig. 1, maps covering the $[50^\circ\text{S} - 70^\circ\text{S}]$ area. For all runs, a dominant trend of
185 positive bias can be identified in the Southern Ocean, with the highest values in the Pacific
186 Southern Ocean. Negative biases of SWH are also observed in the Atlantic and Indian ocean near
187 the Marginal Ice Zone (MIZ), where strong uncertainties are expected on local winds related to
188 sea-ice melt-water. There is an evident bias reduction when satellite data are assimilated. On
189 average, the control run (without assimilation) leads to a mean bias for SWH of approximately
190 0.13 m (Fig. 1d) with maximum values reaching 1 m. The mean bias reduces to 0.10 m when
191 assimilating satellite SWH estimates (Fig. 1b). Incorporating wavenumbers in the assimilation
192 further significantly contributes to reduce the bias, dropping to 0.03 m for assimilation of

193 wavenumbers only (Fig. 1a), and 0.05 m, when assimilating both wavenumbers and SWH (Fig.
194 1c). The slight increase in bias in run C can be explained by the use of empirical power laws for
195 wave growth (Lionello et al. 1992) to redistribute the corrections from assimilating SWH over
196 the full wave spectrum. This reduces the benefit of directly correcting the partition (dominant
197 wave train). In addition, the weight of the assimilation of SWH in run C is greater because of the
198 higher resolution of the observations (every ~ 7 km compared to 70 km for partitions).



199

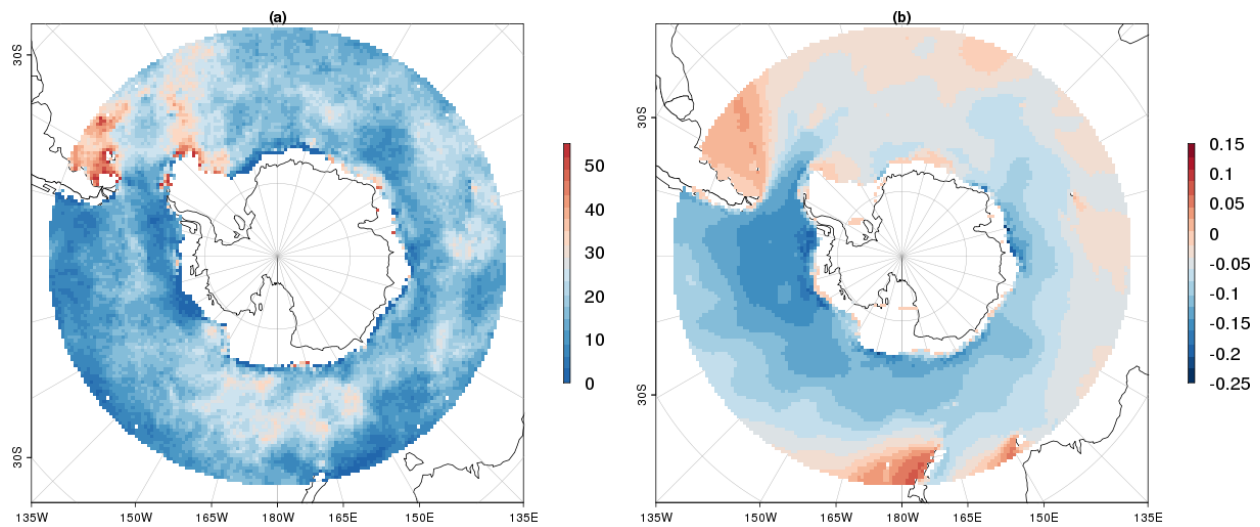
200 **Figure 1.** Bias maps of SWH (in cm) for simulations of the MFWAM model in comparison with
201 altimeters Jason-3, Saral/Altika and Sentinel-3 during the period starting from 26 April to 1 June
202 2019. (a), (b), (c) and (d) indicate runs A, B, C and D, respectively.

203 To explore the impact of the assimilation on high waves generated by heavy storm conditions, a
204 scatter analysis from MFWAM and altimeter sensors is performed for selected SWH larger than
205 5 m, which are mostly located in the Pacific sector (about 11071 points). Overall, run A results in
206 an excellent correlation with altimeter data, with scatter diagram following the slope 1:1 and
207 intercept of 0.04m, substantiating the significant bias reduction. On the contrary, run B shows an
208 overestimation of model results, with data points distributed along a slope of 1.05, intercept of -

209 0.19 m and a mean positive bias of 0.11 m. For run C the slope and the intercept are 1.03 and -
210 0.14, which show the improvement induced by the assimilation of wavenumbers compared to
211 run B. In terms of Normalized Root Mean Square Error (NRMSE), the best performance for
212 large SWH (greater than 5m), 10.3%, is obtained when assimilating wavenumber components
213 (runs A and C). For the assimilation of SWH only and the control run, NRMSE are about 10.6%
214 and 11%, respectively.

215 To explain this result, it must be recalled that in the wind wave growth phase, there is a transfer
216 of wave energy from the high frequencies to the smaller frequencies, until an equilibrium state is
217 reached. In general, the wind input term in a wave model which describes the wave growth
218 depends, for each frequency, upon the difference between wave and wind directions. The fact
219 that the assimilation of wavenumber components corrects both the wave direction and the
220 dominant frequency directly leads to improved wave growth and the energy transfer for wind
221 waves before the equilibrium state.

222 Also, recall that the wave age, expressed as the ratio of peak wave phase speed C_p and the
223 surface wind speed U_{10} , indicates whether the sea state is windsea or swell dominant. The
224 windsea can therefore be identified by a wave age C_p/U_{10} lower than 1.2. Figure 2a shows the
225 regional distribution of wind sea, by the probability of occurrence associated with a wave age
226 smaller than 1.2 (estimated over the analyzed period). In general swell is dominant in the
227 Southern Ocean; however there are several regions where the occurrence of wind sea is
228 important (30-50%) like in the western sector of the Atlantic and Pacific ocean. This is due to the
229 occurrence of relatively close storm systems, which limits fetches for wave growth.

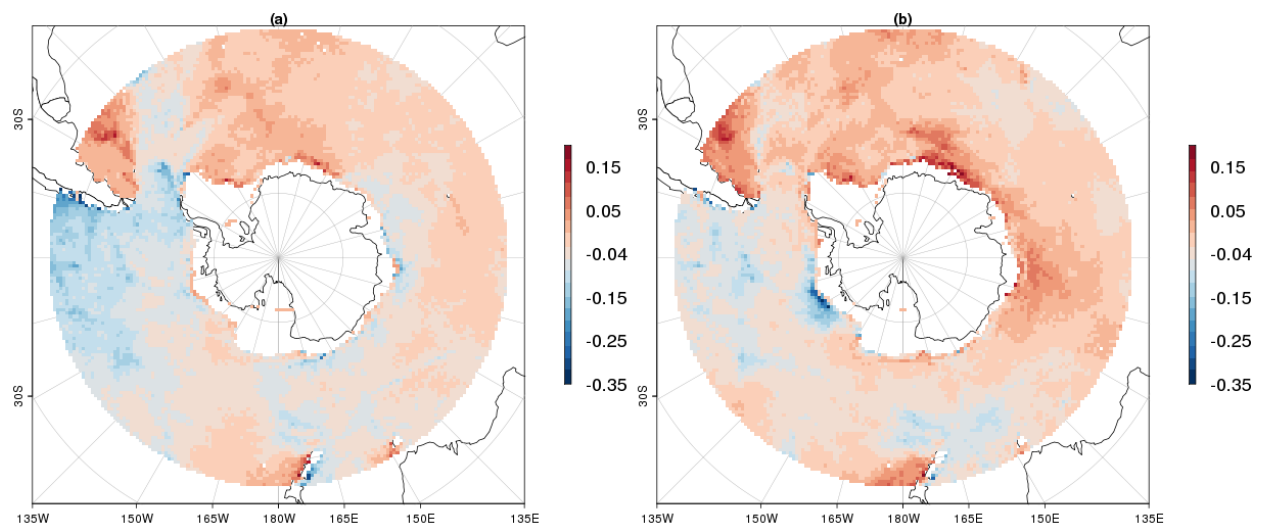


230
231 **Figure 2.** (a) Probability of occurrence (color code indicates percentage) of dominant windsea
232 sea state ($C_p/U_{10} < 1.2$) from model run A. (b) mean difference of SWH between run A and run D
233 during the period from 26 April to 1 June 2019.

234 Elsewhere, the low probability of wind sea (i.e. predominance of swell) indicates the
235 presence of fully-developed waves or swell, for instance in the Drake passage, Chile sector.
236 Figure 2b shows the difference between the mean SWH derived from model runs with

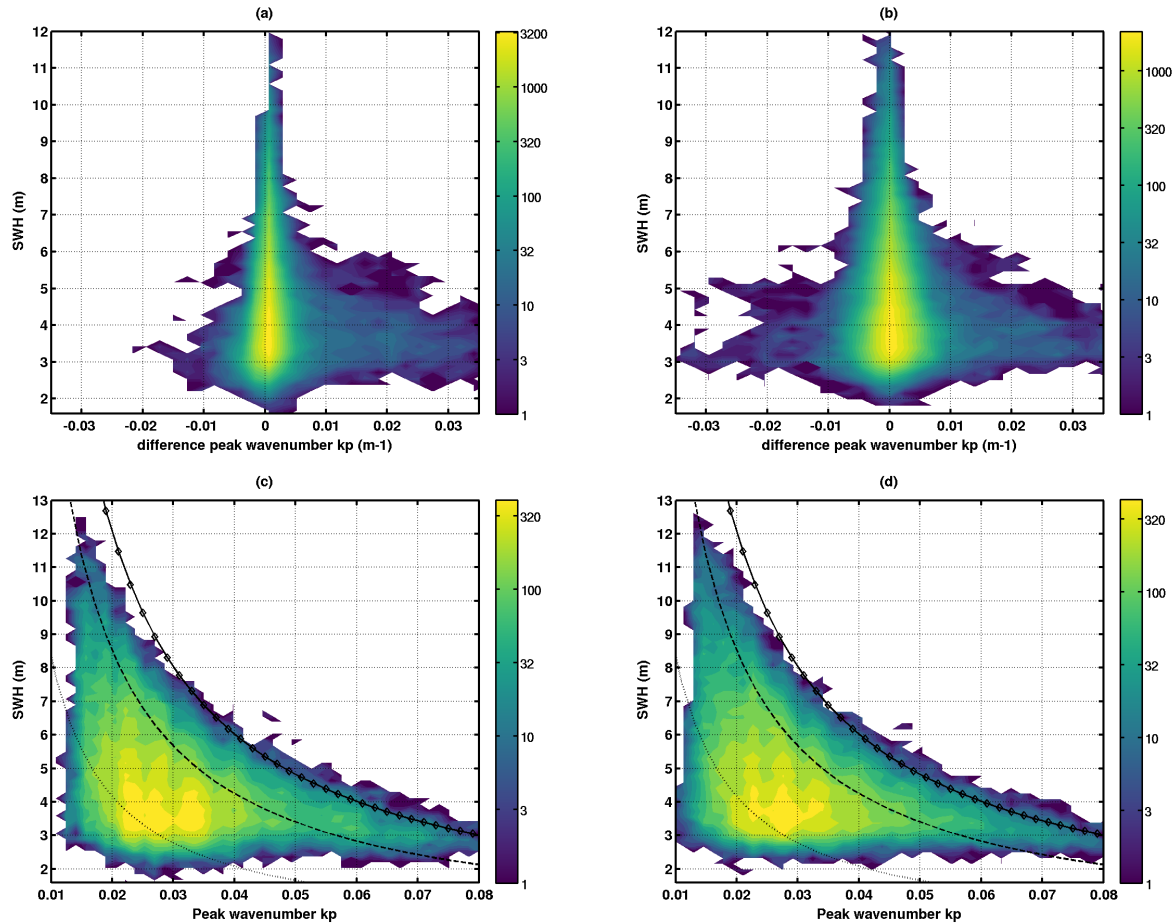
237 assimilation of partition wavenumber components (run A) and benchmark simulation (run D).
238 The assimilation results in a significant reduction of the significant wave height throughout the
239 western part of the Southern Ocean in comparison with the control run. The extent of this
240 difference depends on the wave age (cf. Figure 2a). Small differences are reported in the Atlantic
241 Ocean and Indian Ocean Sector, where swell is not dominant (cf. Fig. 2a), while the largest
242 average differences—up to -0.25 m—are found in the Pacific Ocean sector, especially in the
243 Amundsen Sea and Bellingshausen Sea subsectors and in the Drake passage. There are the areas
244 where the wind sea generated South of New Zealand has transformed into a swell after a long,
245 uninterrupted propagation.

246 Let's define the difference between assimilation runs and the control run the analysis
247 increment. The impact of run A on the peak wave age indicates two trends on the analysis
248 increment as shown in Figure 3a. The first trend concerns the Pacific Ocean sector and Drake
249 Passage where there is a strong negative analysis increment on average which is linked to the
250 overestimation of the wave age by the run D. The average difference in this sector reaches -0.25.
251 The second trend is observed in the Atlantic and Indian oceans sectors where we see that the
252 assimilation of partitions wavenumbers induces a positive increment. This latter indicates an
253 underestimation of the wave age by the control run D with a maximum average difference of
254 0.15. By comparing figures 3a and 3b we see that run B mainly indicates positive increments in
255 all sectors and enhanced in some regions the impact in comparison with run A. The negative
256 increment caused by run B is limited and not significant correction. This can be explained by the
257 use of empirical power laws (Lionello et al. 1992) which seems less efficient to correct peak
258 wave age in unlimited fetch conditions in Pacific sector of the Southern Ocean.



260 **Figure 3.** Average of difference of wave age (C_p/U_{10}) of runs with and without assimilation
261 during the period between 26 April and 1 June 2019. (a) stand for the assimilation of
262 wavenumber components (run A), while (b) indicate the assimilation of SWH only. Negative
263 values mean overestimation of wave age and conversely positive values indicate underestimation
264 of the control run.

265



266

267 **Figure 4.**(a,b): variation of analysis increment of peak wavenumber with SWH, for model runs
 268 A and B, respectively. (c,d): Relation between SWH peak wavenumber with, for model runs A
 269 and B., respectively. The dotted, dashed and diamond lines indicate the theoretical variation for
 270 peak wavenumber of young (wave age=0.7), mature (wave age=1) and fully developed (wave
 271 age=1.2) seas according to the wave spectrum model of Elfouhaily et al. (1997). With equations
 272 (37) and (38) in Elfouhaily et al.(1997), we obtained the following relation $SWH=(0.17/k_p)*\Omega^{-1.7}$
 273 where Ω is the inverse wave age. Color bars indicate the density of points by pixel.

274 To investigate the difference between run A and run B we analyzed the analysis increment of
 275 dominant wavenumbers from these two runs in comparison with the control run D. Figure 4a and
 276 4b show the analysis increment of the dominant wavenumber of runs A and B, respectively, as a
 277 function of SWH located on the altimeters tracks used for the bias evaluation in the Southern
 278 Ocean. Clearly, the assimilation of the partition wavenumbers mainly leads to a positive
 279 correction of the dominant wavenumber k_p (Fig.4a), which indicates an underestimation of the
 280 control run D. This increase of the wave number is most pronounced for high SWH (larger than
 281 5 m), which shows that assimilation maintains the wave regime in the growth phase. Figure 4c
 282 reveals that the majority of the dominant wavenumbers k_p points are between the theoretical
 283 curves of young and mature seas as given by the Elfouhaily spectrum (Elfouhaily et al., 1997).
 284 Figure 4c further indicates a good consistency of the variation of dominant wavenumber with
 285 SWH in comparison with theoretical curves. On the contrary for run B (Fig. 4b) , we notice that

286 the correction of k_p is dominated by negative analysis increments for strong SWH (larger than 5
287 m). This explains the difficulty of run B to reduce the bias for large SWH, and also to improve
288 the dominant wavenumbers during the growth phase. Figure 4d also indicates that the number of
289 k_p points between the young and mature sea curves is smaller compared to Figure 4c.

290 5 Discussions

291
292 The peak group velocity (C_g) of waves for deep water depends on peak wave number, as
293 $0.5*(g/k_p)^{0.5}$, where g is the gravity acceleration. The non-linear interactions govern the peak
294 frequency downshift as long as the waves are young. The process of wave growth in storm
295 systems is then closely related to the fetch and wind duration conditions. Studies (e.g. Hsu et al.
296 2019, Kudryatsev et al. 2015) have evidenced the dependency between the wave group velocity
297 (C_g) and storm displacement speed (V). For extra-tropical storms and based on self-similarity
298 theory (Badulin et al. 2007), Kudryatsev et al. (2015) proposed a limiting condition of the wave
299 group velocity, independent of wind speed, $C_{g_max} = V/(1 + q)$, where q depends on fetch laws.
300 Considering JONSWAP growth conditions (Hasselmann et al. 1976), $q=-3/10$, it leads to
301 $C_{g_max}=10/7*V$. Mature waves outrunning rapid extra-tropical storms are thus expected to
302 reach large wavelengths and group velocities, independent of the maximum wind conditions.
303 Today, this effect is not well taken into account in numerical wave models and errors in the
304 velocity of storm displacement may impact significantly the modeled wave field. For severe
305 storms the winds from atmospheric models are in general underestimated, and this is
306 compensated by a larger wind action and slower velocity of storm displacement. In consequence
307 the wave model controlling the non-linear interactions (fetch laws) with ad-hoc adjustments
308 between wind-wave growth and wave breaking dissipation can partly reduce the misfit of the
309 wind, but this is accompanied by enhance wave growth. This relation between C_g and V
310 thus highlights the key advantage of assimilating observations of directional wave numbers.
311 To explore the quantitative impact of the assimilation of wavenumbers on C_g in the Southern
312 Ocean we considered the points used in the validation with altimeters under wind sea wave
313 regime (about 25170 points corresponding to ~4% of the total). During the period of study the
314 mean and maximum C_g for run A are about 7.5 and 13.1 m/s, respectively, whereas they are 7.7
315 and 15.1 m/s, respectively for run D. This indicates that in the mean, the assimilation of
316 wavenumbers partitions reduced the overestimation of C_g by the model. By analyzing the
317 distribution of the difference of C_g between runs A and D, the correction of underestimation of
318 C_g concerns 26% of the points, while the correction of overestimation of C_g is about 64% of the
319 points. Thus the assimilation wavenumbers helps control C_g directional properties during growth
320 phase and evolution within and outside the large and rapid storms in the Southern Ocean, which
321 favor trapping fetch conditions as described by Kudryatsev et al. (2015) or Hsu et al. (2019) for
322 tropical or mid-latitude storms. It is worth mentioning that corrections on C_g impact the wave
323 steepness and related dissipation from wave breaking, which in turn modulates the upper ocean
324 turbulence and mixing conditions. The decrease in C_g and related increase of wave steepness
325 sustains the wind sea growth phase with enhanced non-linear interactions.
326 In summary, the assimilation of wavenumbers partitions induces a significant reduction in SWH
327 bias during the wave growth phase in the Southern Ocean. This is accompanied by a correction
328 on the dominant wavenumber and wave age. The impact on group velocity indicates a change in
329 the relative velocity between wave groups and storm displacement, which can result in an
330 enhancement of the wave energy and wave breaking that affects the ocean mixing layer and air-

331 sea interaction. The assimilation of wave number partitions shed lights on difficulties related to
332 wind-wave generation in the wave model. This opens the development of better parametrizations
333 to storm conditions in the Southern Ocean.
334

335 **6 Conclusions**

336 The Southern Ocean is dominated by strong wave systems which can strongly modulate
337 air-sea interactions and ocean and sea-ice dynamics (e.g. Humphries et al. 2016; Schamle et al.
338 2019, Thurnherr et al. 2020, Vichi et al. 2019, Alberello et al. 2020). Contemporary wave models
339 generally provide biased estimates of the significant wave height in this region, despite
340 assimilation of satellite observations. However, assimilation methods are limited to significant
341 wave height or truncated directional wave energy spectra, to mostly account for swell systems,
342 but neglecting the short wave components of the wind sea. With the instrument SWIM carried by
343 the CFOSAT satellite, it is now possible to more systematically detect directional wave
344 propagation properties that resolve both swell and wind-wave systems. This study demonstrates
345 that the assimilation of these directional wavenumber components from more comprehensive
346 spectra enhances model prediction of energy transfer during the wave growth phase. This leads
347 to improved estimation of the significant wave height in the Southern Ocean. The validation is
348 conducted by comparing significant wave height from model runs with and without assimilation
349 against observations from altimeter sensors. Overall, all data assimilation reduces biases.
350 However, model runs with assimilation of wavenumber components (i.e. directional properties)
351 are the most efficient with substantial bias reduction (from 13 cm bias without assimilation to
352 3cm with assimilation) compared to assimilation of significant wave height only.

353 Results show that taking into account wavenumbers components can significantly
354 correct the wave age and the dominant wavenumber in the Southern Ocean, to help control the
355 transition between wind waves and mature sea regimes. This is verified with the theoretical
356 growth curves (SWH as function with k_p). Overall, we observe a better spread of the impact on
357 wave age when using directional observations around the Southern Ocean in comparison with
358 the assimilation of significant wave height only. The transition to swell regime and the
359 propagation in the northern ocean region is also well tracked as it is observed in Pacific Ocean
360 sector. Clearly, the assimilation of SWH only showed a limited and only localized impact on the
361 wave age.

362 This research opens perspectives on the use of the directional capabilities of SWIM
363 instrument on-board of the CFOSAT mission to improve wave model forecast. The assimilation
364 of wave number components is promising and expected to improve the descriptions of
365 ocean/atmosphere coupling in terms of both momentum and gas flux transfer in the Southern
366 Ocean, which are still poorly understood in climate models.

367 **Acknowledgments and data**

368 This work is funded by the French Space Agency CNES in the frame of TOSCA national
369 program. The level 2 data used here are processed by SWIM algorithms version V5.0.1. The
370 quality controlled data are accessible on shared research depository zenodo following this URL

371 web link : <https://doi.org/10.5281/zenodo.4392511> . The authors would also like to thank Alice
372 Dalphinnet and Malek Ghantous for helping to the preparation of the manuscript.
373

374 **References**

- 375 Alberello, A., Bennetts, L., Heil, P., Eayrs, C., Vichi, M., MacHutchon, K., Onorato, M. &
376 Toffoli, A.: Drift of Pancake Ice Floes in the Winter Antarctic Marginal Ice Zone During Polar
377 Cyclones, *Journal of Geophysical Research: Oceans*, 125, e2019JC015 418,
378 doi.org/10.1029/2019JC015418, 2020.
- 379 Aouf L., Dalphinnet, A., Hauser, D., Delaye, L., Tison, C., Chapron, B., Hermozo, L., & Tourain,
380 C. (2019), On the Assimilation of CFOSAT Wave Data in the Wave Model MFWAM :
381 Verification Phase, proceedings of IGARSS 2019 - IEEE International Geoscience and Remote
382 Sensing Symposium, Yokohama, Japan, 2019, pp. 7959-7961, doi:
383 [10.1109/IGARSS.2019.8900180](https://doi.org/10.1109/IGARSS.2019.8900180).
- 384 Aouf L. & Lefèvre J-M. (2015), On the impact of the assimilation of SARAL/Altika wave data
385 in the operational wave model MFWAM, *Marine Geodesy*, 38, 381-395.
386 [doi:10.1080/01490419.2014.1001050](https://doi.org/10.1080/01490419.2014.1001050)
- 387 Aouf, L., Lefèvre, J-M. & Hauser D. (2006), Assimilation of directional wave spectra in the
388 wave model WAM: An impact study from synthetic observations in preparation for the
389 SWIMSAT Satellite mission. *J Atmos Ocean Technol.* doi: [10.1175/JTECH1861.1](https://doi.org/10.1175/JTECH1861.1)
- 390 Ardhuin, F., Rogers, E., Babanin, A., Filippot, J-F., Magne, R., Roland, A., Van Der
391 Westhuysen, A.; Queffeuilou, P., Lefèvre, J-M., Aouf, L. & Collard, F. (2010), Semi empirical
392 Dissipation Source Functions for Ocean Waves. Part I: Definition, Calibration, and Validation. *J.*
393 *Phys. Oceanogr.*, **40**, 1917–1941, doi:[10.1175/2010JPO4324.1](https://doi.org/10.1175/2010JPO4324.1).
- 394 Babanin A. V., Rogers, E. W., de Camargo, R., Doble, M., Durrant, T., Filchuk, K., Ewans, K.,
395 Hemer, M., Janssen, T., Kelly-Gerreyn, B., Machutchon, K., McComb, P., Qiao, F., Schulz, E.,
396 Skvortsov, A., Thomson, J., Vichi, M., Violante-Carvalho, N., Wang, D., Waseda, T., Williams,
397 G. & Young, I. R. (2019) Waves and swells in high wind and extreme fetches, measurements in
398 the Southern Ocean, *Frontiers in Marine Science*, 6, 361, DOI:[10.3389/fmars.2019.00361](https://doi.org/10.3389/fmars.2019.00361)
- 399 Badulin, S. I., Babanin, A. V., Zakharov, V. E., & Resio, D. (2007), Weakly turbulent laws of
400 wind-wave growth, *J. Fluid Mech.*, 591, 339–378, doi:[10.1017/S0022112007008282](https://doi.org/10.1017/S0022112007008282).
- 401 Barbariol, F., Benetazzo, A., Bertotti, L., Cavaleri, L., Durrant, T., McComb, P., & Sclavo, M.:
402 Large waves and drifting buoys in the Southern Ocean, *Ocean Engineering*, 172, 817–828, 2019
- 403 Chapron, B., Johnsen, H. & Garello, R. (2001), Wave and wind retrieval from SAR images of
404 the ocean, *Ann. Telecommun.* 56, 682–699 (2001). <https://doi.org/10.1007/BF02995562>
- 405 Collard F., Ardhuin, F. & Chapron, B. : Monitoring and analysis of ocean swell fields from space
406 : New methods for routines observations, *Journal of Geophysical Research*,
407 [10.1029/2008JC005215](https://doi.org/10.1029/2008JC005215), 14, issue C7, 2005
- 408 ECMWF (2013) Part VII : IFS Documentation CY38R1, Part VII ECMWF Wave Model.
409 <https://www.ecmwf.int/node/9248>
- 410 Ewans K., 1998, Observations of the directional wave spectrum of fetch-limited waves, *J. Phys.*
411 *Oceanogr.*, **28**, 498–512.
- 412 Donelan, M. A., Hamilton, J. & Hui, W. H. (1985) : Directional spectra of wind-generated waves.
413 *Philos. Trans. Roy. Soc. London.*, **A315**, 509–562.

- 414 Elfouhaily, T., Chapron, B., Katsaros, C. & Vandemark, D. : A unified directional spectrum for
415 long and short wind-driven waves. *Journal of Geophysical Research*, Volume 102, C7,
416 <https://doi.org/10.1029/97JC00467>.
- 417 Fadaeiazar, E., Leontini, J., Onorato, M., Waseda, T., Alberello, A. & Toffoli, A.: Fourier
418 amplitude distribution and intermittency in mechanically generated surface gravity waves, *Phys.*
419 *Rev. E*, 102, 013 106, doi.org/10.1103/PhysRevE.102.013106, 2020
- 420 Gunther, H., Rosenthal, W. & Dunckel, M., (1981), The response of surface gravity waves to
421 changing wind direction, *Journal of Physical Oceanography*, 11, 718-728,
422 [https://doi.org/10.1175/1520-0485\(1981\)11<718:RSGW>2.0.CO;2](https://doi.org/10.1175/1520-0485(1981)11<718:RSGW>2.0.CO;2)
- 423 Humphries, R. S., Klekociuk, A. R., Schofield, R.,
424 Keywood, M., Ward, J. & Wilson, S. R.: Unexpectedly high ultrafine aerosol concen-385trations
425 above East Antarctic sea ice, *Atmos. Chem. Phys.*, 16, 2185–2206, [doi.org/10.5194/acp-16-2185-](https://doi.org/10.5194/acp-16-2185-2016)
426 2016, 2016.
- 426 Gerling, T. W., Partitioning sequences and arrays of directional ocean wave spectra into
427 component wave systems, *J. Atmos. Oceanic Technol.*, 9, 444– 458, 1992.
- 428 Hasselmann K., P. T. Barnett, E. Bouws, H. Carlson, E. D. Cartwright, K. Enke, A. J. Ewing, H.
429 Gienapp, E. D. Hasselmann, P. Kruseman, A. Meerburg, P. Muller, D. Olbers, K. Richter, W.
430 Sell, & H. Walden. Measurements of wind-wave growth and swell decay during the joint north
431 sea wave project (JONSWAP). *Deut. Hydrogr. Z.*, 8 : 1–95, 01 1973.
- 432 Hasselmann, D. E. & Dunckel, M. & Ewing, J. A. (1980) : Directional wave spectra observed
433 during JONSWAP 1973. *J. Phys. Oceanogr.*, **10**, 1264–1280.
- 434 Hasselmann K., Chapron B., Aouf L., Arduin F., Collard F., Engen G., Heimbach P., Janssen
435 P., Krogstad H., Lehner S., Li J-G., Li Xiaoming, Rosenthal W. & Schulz-Stellenfleth J. (2012) :
436 The ERS SAR Wave Mode – A Breakthrough in global ocean wave observations. European
437 Space Agency, (Special Publication) ESA SP. 1326.
- 438 Hasselmann, K., Ross, D. B., Muller, P., & W. Sell (1976): A parametric wave prediction model,
439 *J. Phys. Oceanogr.*, 6, 200–228, [doi:10.1175/1520-0485\(1976\)006](https://doi.org/10.1175/1520-0485(1976)006)
- 440 Hauser D., et al., "New Observations From the SWIM Radar On-Board CFOSAT: Instrument
441 Validation and Ocean Wave Measurement Assessment," in *IEEE Transactions on Geoscience*
442 *and Remote Sensing*, doi: 10.1109/TGRS.2020.2994372.
- 443 Hsu, J.-Y., Lien, R.-C., D'Asaro, E. A., & Sanford, T. B. (2019). Scaling of drag coefficients
444 under five tropical cyclones. *Geophysical Research Letters*, 46, 3349–3358.
445 <https://doi.org/10.1029/2018GL081574>
- 446 Kudryavtsev, V., P. Golubkin, P., & Chapron, B. (2015), A simplified wave enhancement
447 criterion for moving extreme events, *J. Geophys. Res. Oceans*, 120, 7538–7558,
448 [doi:10.1002/2015JC011284](https://doi.org/10.1002/2015JC011284).
- 449 Le Traon P. Y., Reppucci A. & Alvarez Fanjul E. et al (2019) From Observation to Information
450 and Users: The Copernicus Marine Service Perspective. *Front Mar Sci.* doi:
451 [10.3389/fmars.2019.00234](https://doi.org/10.3389/fmars.2019.00234)
- 452 Lionello, P., Gunther, H. & Janssen, P. A. E. M. (1992). Assimilation of altimeter data in a
453 global third generation wave model. *J. Geophys. Res.*, C97, 14453–14474.
- 454 Long, C. E. & Resio, D. (2007). Wind wave spectral observations in Currituck Sound, North
455 Carolina. *J. Geophys. Res.* 112, CO5001.
- 456 Mitsuyasu, H., Tasai, F., Sahara, T., Mizuno, S., Ohkusu, M., Honda, T. & Rikiishi, K. & (1975).
457 Observations of the directional spectrum of ocean waves using a clover leaf buoy. *J. Phys.*
458 *Oceanogr.* 5, 750–760.

- 459 Pierson, W. J., & Moskowitz, L., A proposed spectral form for fully developed wind sea based
460 on the similarity theory of S. A. Kitaigorodskii, *J. Geophys. Res.*, 69, 5181-5190, 1964.
- 461 Phillips, O. M., *The Dynamics of the Upper Ocean*, 2nd ed., Cambridge Univ. Press, New York,
462 1977.
- 463 Resio D. T., Linwood V. & Ardag D., Characteristics of directional wave spectra and
464 implications for detailed-balance wave modeling, *Ocean Modelling*, doi:10.1016/j.ocemod.
465 2015. 09.009
- 466 Schmale, J., Baccarini, A., Thurnherr, I., Henning, S., Efraim, A., Regayre, L., Bolas, C.,
467 Hartmann, M., Welti, A., Lehtipalo, K., Aemisegger, F., Tatzelt, C., Landwehr, S., Modini, R. L.,
468 Tummon, F., Johnson, J. S., Harris, N., Schnaiter, M., Toffoli, A., Derkani, M., Bukowiecki, N.,
469 Stratmann, F., Dommien, J., Baltensperger, U., Wernli, H., Rosenfeld, D., Gysel-Ber, M. &
470 Carslaw, K. S.: Overview of the Antarctic Circumnavigation Expedition: Study of Preindustrial-
471 like Aerosols and Their Climate Effects (ACE-SPACE), *Bull. Am. Meteorol. Soc.*, 100, 2260–
472 2283, doi.org/10.1175/BAMS-D-18-0187.1, 2019.
- 473 Thurnherr, I., Kozachek, A., Graf, P., Weng, Y., Bolshiyarov, D., Landwehr, S., Pfahl, S.,
474 Schmale, J., Sodemann, H., Steen-Larsen, H. C., Toffoli, A., Wernli, H. & Aemisegger, F.:
475 Meridional and vertical variations of the water vapour isotopic composition in the marine
476 boundary layer over the Atlantic and Southern Ocean, *Atmos. Chem. Phys.*, 20, 5811–5835,
477 doi.org/10.5194/acp-20-5811-2020, 2020
- 478 Toffoli, A., Proment, D., Salman, H., Monbaliu, J., Frascoli, F., Dafilis, M., Stramignoni, E.,
479 Forza, R., Manfrin, M. & Onorato, M., 2017, Wind Generated Rogue Waves in an Annular
480 Wave Flume, *Phys. Rev. Letters*, 118, issue 14, 10.1103/PhysRevLett.118.144503.
- 481 Toffoli, A., Onorato, M., Bitner-Gregersen, E. M. & Monbaliu, J. (2010). Development of a
482 bimodal structure in ocean wave spectra. *J. Geophys. Res.* 115.
- 483 Vichi, M., Eyras, C., Alberello, A., Bekker, A., Bennetts, L., Holland, D., de Jong, E., Joubert,
484 W., MacHutchon, K., Messori, G., Mojica, J. F., Onorato, M., Saunders, C., Skatulla, S. &
485 Toffoli, A.: Effects of an explosive polar cyclone crossing the Antarctic marginal ice zone,
486 *Geophys. Res. Lett.*, 46, 5948–5958, 2019.
- 487 Young, I. R. 1999: Seasonal variability of the global ocean wind and wave climate, *Int. J.*
488 *Climatol.*, 19, 931-950, doi:10.1002/(SICI)1097-0088(199907)19:9<931
- 489 Young, I. R., Fontaine, E., Liu, Q., & Babanin, A. V.: The Wave Climate of the Southern Ocean,
490 *J. Phys. Oceanogr.*, 50, 1417–1433, 2020.
- 491 Young I. R., Verhagen, L. A. & Banner, M. L. (1995) : A note on the bimodal directional
492 spreading of fetch-limited wind waves. *J. Geophys. Res.*, 100 (C1), 773–778.
- 493 Zieger, S., Babanin, A. V., Rogers, W. E. & Young, I. R.: Observation-based source terms in the
494 third-generation wave model WAVE-WATCH, *Ocean Modelling*, 96, 2–25, 2015.